U-Center-Induced Raman Scattering in KBr and KI†

G. Paul Montgomery, Jr.,* W. R. Fenner,‡ and M. V. Klein
Department of Physics and Materials Research Laboratory, University of Illinois, Urbana, Illinois 61801

and

Thomas Timusk
Department of Physics, McMaster University, Hamilton, Ontario, Canada

Raman scattering from the second harmonic state of the high-frequency *U*-center localized mode has been measured in KBr:H^-, KBr:D^-, KI:H^-, and KI:D^- at 10 K. Lines of A_{1g}, E_g, and T_{2g} symmetry are observed. The peak positions and symmetries of these lines are in agreement with the static-lattice model of the local mode. The anharmonic coupling coefficients needed to calculate the localized oscillator energy levels have been determined from the experimental data and used to describe the short-range repulsive potential in the neighborhood of the *U* center. The importance of polarization effects in the interaction of the impurity with its surroundings is demonstrated. A weak peak of A_{1g} symmetry has been observed in KI:H^- at about 95 cm^{-1}. It is attributed to a gap mode previously seen in infrared sideband measurements. Absolute Raman-scattering efficiencies and cross sections have been determined for all the impurity-induced modes in KI:H^-, and the polarizability derivatives associated with the gap mode have been computed.

I. INTRODUCTION

In 1960 Schaefer[1] observed that *U* centers (substitutional H^- ions) in alkali halides produce infrared-absorption bands at frequencies well above the maximum host-lattice phonon frequency. This discovery stimulated considerable interest in the lattice dynamics of crystals containing these impurities. Rosenstock and Klick[2] and Wallis and Maradudin[3] demonstrated that the band was due to a strongly localized vibrational mode of the H^- ion. Early calculations[3,4] assumed that the *U* center could be treated as a simple mass defect. As long as only nearest-neighbor short-range forces were considered, these calculations agreed well with experiment. However, when long-range electrostatic forces were taken into account, it was shown by Jaswal and Montgomery[5] using the rigid-ion and deformation-dipole models, by Fieschi, Nardelli, and Terzi[6,7] using the shell model, and by Page and Strauch[8] using the breathing-shell model, that the central-force constant between the impurity and its nearest neighbors had to be decreased by about 50% to obtain agreement with experiment.

In addition to the main *U*-center absorption band, Schaefer[1] also observed sidebands. Fritz[9] first proposed that these were caused by anharmonic coupling between the local mode and perturbed band modes. These sidebands have received considerable theoretical and experimental study.[10–25]

Symmetry considerations show that the perturbed band modes which appear as sidebands must have A_{1g}, E_g, or T_{2g} symmetry. Hence they should be observable directly by Raman scattering. Although several authors have calculated theoretically the Raman spectra to be expected from substitutional H^- ions,[26,27] all attempts to observe *U*-center-induced Raman scattering in alkali halides have been singularly unsuccessful. (However, Harrington *et al.*[28] have successfully observed *U*-center-induced Raman scattering in the alkaline-earth fluorides.)

This paper is a report of the first successful measurement of Raman scattering from *U* centers in alkali halides. We have observed second harmonics of the infrared-active high-frequency localized mode in crystals of KBr and KI doped with H^- and D^- impurities. We have also made a detailed investigation of KI:H^- in the low-frequency region where the even-parity modes of the sideband spectrum are expected to occur. There we have observed a weak scattering peak of A_{1g} symmetry; this peak is attributed to a *U*-center-induced vibrational mode whose frequency lies in the gap between the acoustic and optical branches of the host KI crystal. We have measured the absolute Raman-scattering efficiencies and cross sections for all the impurity peaks, and have estimated the polarizability derivatives associated with the gap mode.

Before presenting the experimental results, we describe in Sec. II a theoretical model for the high-frequency localized mode of the *U* center and its implications for Raman scattering. Experimental procedures and results will be presented in Secs. III, IV, VI, and VII. In Sec. V we use the results of our Raman measurements to describe the short-range interaction between the *U* center and its

nearest neighbors.

II. MODEL FOR LOCALIZED MODE

In dealing with the high-frequency U-center localized mode in the alkaline-earth fluorides, Elliott *et al.*[10] treated the U center as a particle in a static anharmonic potential having the symmetry of the host lattice at the impurity site. This approach is physically reasonable since, during one period of oscillation of its neighbors in a host-crystal band mode, the U center makes many complete oscillations, so that during any one of them, it sees the surrounding ions as essentially at rest. We will see that, at least as far as peak positions are concerned, this model provides a good description of our Raman-scattering data.

In an alkali halide, a substitutional H^- ion is in equilibrium at a site of cubic (O_h) symmetry. Expanding the potential energy in a power series in the displacements of the U center from equilibrium and keeping only terms consistent with this site symmetry, we write the potential energy as

$$V = \tfrac{1}{2} M' \Omega^2 + C_1(x^4 + y^4 + z^4) + C_2(x^2y^2 + y^2z^2 + z^2x^2) , \tag{1}$$

where M' is the impurity mass. This potential energy will be discussed at length in Sec. V.

If we consider the anharmonic terms to be a small perturbation, the unperturbed wave functions are those of a spherically symmetric harmonic oscillator, having energy levels

$$E_n = (n + \tfrac{3}{2})\hbar\Omega . \tag{2}$$

The ground state ($n = 0$) and the first excited state ($n = 1$) are unsplit but shifted by the anharmonic perturbation, and transform, respectively, according to the A_{1g} and T_{1u} irreducible representations of the point group O_h. The sixfold degenerate $n = 2$ level is split by the perturbation into levels of A_{1g} (nondegenerate), E_g (doubly degenerate), and T_{2g} (triply degenerate) symmetry. These energy levels are shown schematically in Fig. 1.

Because of inversion symmetry about the defect site, only transitions between states of different parity are observed in the infrared; the observed frequency of the infrared-active local mode corresponds to a transition from the A_{1g} ground state to the T_{1u} first excited state. Conversely, one expects to observe transitions between the ground state and the A_{1g}, E_g, and T_{2g} second-harmonic states by Raman scattering.

Elliott *et al.*[10] have calculated explicit expressions for the perturbed energy levels relative to the unperturbed ground state. These results are also included in Fig. 1.

Since there are three unknown constants, viz., C_1, C_2, and Ω, and three allowed Raman transitions, the complete energy-level scheme for the U center can be determined from the Raman data provided all the predicted lines are observed. This point is discussed further in conjunction with the experimental results in Sec. IV.

III. EXPERIMENTAL PROCEDURE

The preparation of the doped KBr and KI crystals used in this investigation has been described previously.[11] The impurity concentrations were determined by measuring the integrated absorption strengths of the U-center localized mode. These are tabulated in Table I.

The Raman measurements were made in a metal top-loading cryostat with antireflection-coated Pyrex windows. The sample chamber was isolated from the main vacuum region, and the samples were cooled by filling this chamber with helium exchange gas. Sample temperatures were measured to ± 1 K with a gold + 0.07-at.% iron-vs-copper thermocouple.[29,30]

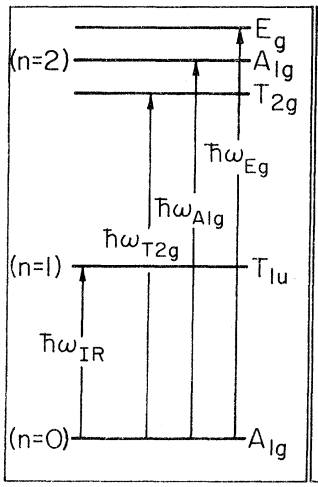

$$E_n(\Gamma) = n\hbar\Omega + \left[\mu_1(\Gamma)\cdot C_1 + \mu_2(\Gamma)\cdot C_2\right]\left(\frac{\hbar}{2M'\Omega}\right)^2$$

n	Γ	$\mu_1(\Gamma)$	$\mu_2(\Gamma)$
0	A_{1g}	9	3
1	T_{1u}	21	7
2	T_{2g}	33	15
	A_{1g}	45	15
	E_g	45	9

FIG. 1. Energy levels of an anharmonic local oscillator in a cubic environment.

TABLE I. *U*-center concentrations in crystals used in this investigation.

	KBr : H^-	KBr : D^-	KI : H^-	KI : D^-
Impurity concentration (number per cm^3)	3.0×10^{18}	4.7×10^{17}	6.7×10^{17}	7.7×10^{17}

The Raman spectra were taken in the usual right-angle scattering geometry using a Spex double monochromator, an ITT FW-130 photomultiplier tube with S-20 response, and an argon laser operating at 4880 Å with approximately 1-W output. A half-wave plate was used for rotating the incident laser polarization, and a polarizing sheet for analyzing the scattered radiation. A polarization scrambler between the polarizing sheet and the monochromator entrance slit ensured that the Raman light entered the spectrometer as unpolarized light. This is important in measurements of absolute efficiencies and cross sections since the response of the monochromator may differ for light polarized parallel and perpendicular to the grating rulings.

In the measurements of KBr : H^-, KBr : D^-, and KI : D^-, the photomultiplier output was measured with a picoammeter and recorded on a chart recorder. Repeated scans were made of each spectrum and the recorder traces were digitized with the aid of an Autotrol and averaged by computer. Photon-counting electronics were used to obtain the KI : H^- spectra in digital form. Data points were taken every 0.2 Å with 100-sec dwell time at each point. The digital output was punched on paper tape by a teletype and processed by computer. The long dwell times possible with the photon-counting system enabled us to take the KI : H^- spectra with considerably narrower slits than those used in the other work; this made possible a significant improvement in resolution, as evident from a comparison of Figs. 2 and 3.

Our samples were cut, polished, and oriented so that the incident laser radiation propagated along a [001] crystal axis and the Raman-scattered light was collected along $[\bar{1}10]$. This orientation enabled us to determine unambiguously the symmetries of all observed Raman lines by recording the spectra as a function of the polarizations of the incident and scattered light. Let $\hat{k}_L$, $\hat{\eta}_L$ and $\hat{k}_S$, $\hat{\eta}_S$ denote the propagation and polarization directions of the incident and scattered light, respectively. Then, for a given crystal orientation, the experimental geometry is uniquely specified by the label $\hat{k}_L(\hat{\eta}_L, \hat{\eta}_S)\hat{k}_S$.[31] In particular, take $x \parallel [110]$, $y \parallel [\bar{1}10]$, and $z \parallel [001]$. Then the $z(xx)y$ geometry shows A_{1g}, E_g, and T_{2g} modes simultaneously, $z(yx)y$ shows only E_g modes, and T_{2g} modes alone are seen in the $z(xz)y$ and $z(yz)y$ orientations.

There is a certain arbitrariness in defining the Raman intensity associated with a given mode, since the observed intensity may vary with crystal orientation or scattering geometry. For definiteness, we define the Raman intensity (or efficiency or cross section) associated with a particular mode as that which would be observed in the following experimental geometry: incident light propagation along [001]; scattered light propagation along [010]; incident light polarization along [100]; and scattered light unanalyzed.

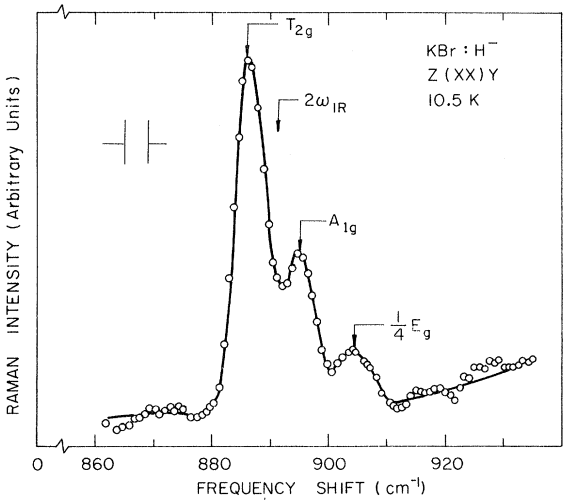

FIG. 2. $z(xx)y$ Raman spectrum of KBr : H^- in second-harmonic region. Here $x \parallel [110]$, $y \parallel [\bar{1}10]$, and $z \parallel [001]$ and frequency is measured in wave-number units.

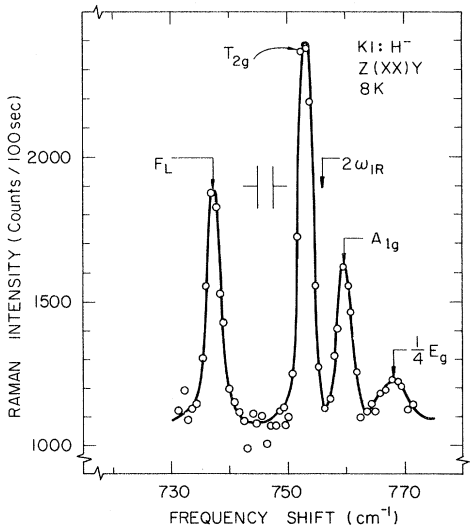

FIG. 3. $z(xx)y$ Raman spectrum of KI : H^- in second-harmonic region. Here $x \parallel [110]$, $y \parallel [\bar{1}10]$, and $z \parallel [001]$ and frequency is measured in wave-number units.

IV. EXPERIMENTAL RESULTS AND DISCUSSION–SECOND HARMONICS

The $z(xx)y$ Raman spectra of KBr : H^- and KI : H^- in the second-harmonic region are shown in Figs. 2 and 3. The spectrometer resolution in each case is indicated. Three lines are observed in each figure, and their symmetries, as determined by $z(xz)y$ and $z(yx)y$ measurements, are in agreement with the theoretical predictions of Sec. II. (The sharp line marked F_L in Fig. 3 is a nonlasing fluorescence line from the argon laser.) In view of our definition of Raman intensity, the E_g line appears in the $z(xx)y$ spectrum with only $\frac{1}{4}$ of its "true" strength. The A_{1g} and T_{2g} lines, at least, are instrument limited, and the intensities of all the lines are too weak to allow them to be practically studied with the monochromator set for smaller spectral bandpass. None of the lines are visible at liquid-nitrogen temperature, and no attempt was made to study their temperature dependence. The values of the observed peak positions are given in the first three rows of Table II. Because of possible error in the spectrometer drive, the absolute peak positions could be in error by ± 2 cm^{-1}. The splittings between the energy levels can be measured to ± 1 cm^{-1} in KBr : H^- and to ± 0.5 cm^{-1} in KI : H^- where the lines are almost completely separated.

The experimental results for ω_A, ω_E, and ω_T and the expressions for the energy levels given in Fig. 1 have been used to determine the parameters Ω, C_1, and C_2 for KBr : H^- and KI : H^-. These results are given in Table II. They are strongly influenced by the experimental uncertainties in the level splittings. In KBr : H^- we find that Ω is accurate to ± 3 cm^{-1}, whereas the accuracies in C_1, C_2, and the ratio C_2/C_1 are, respectively, ± 13, ± 11, and $+25$, -20%. For KI : H^-, Ω is calculable to ± 2 cm^{-1}, C_1 and C_2 to ± 8 and $\pm 7\%$, respectively, and C_2/C_1 is accurate to $+15$, -10%.

We remark that, at least in KBr : H^-, the ratio C_2/C_1 may be close to -3, the value which would be obtained if only the Coulomb interaction contributed to the quartic anharmonicity. This simply means that the contributions of other terms (cf. Sec. V) in the potential energy to C_1 and C_2 nearly cancel, since individually these contributions are nonnegligible.

Consideration of the energy expressions in Fig. 1 shows that the splittings between the different second-harmonic levels are proportional to $\hbar^2(2M'\Omega)^{-2}$. Since Ω is proportional to $M'^{-1/2}$, we expect that the splittings between any two lines would be reduced by a factor of 2 upon substituting D^- for H^-. The ratio of the observed $T_{2g} - E_g$ splittings in the H^-- and D^--doped crystals is 2.16 for KBr and 1.94 for KI. These results are consistent with the above prediction to within the experimental error in peak position.

Unfortunately, this reduced splitting made it impossible to resolve the three lines in the $z(xx)y$ spectra of the D^--doped crystals (not shown). Consequently, although we did observe the T_{2g} and E_g peaks independently in these samples, the A_{1g} peak position was still unknown. It was not felt that the signal-to-noise ratio was good enough to warrant attempting to find it by subtraction of curves. This made direct evaluation of Ω, C_1, and C_2 impossible for D^- doping. To circumvent this difficulty, the following procedure for handling the D^--doped samples was adopted. It was assumed that C_1 and C_2 were the same in both the H^-- and D^--doped samples. The values of C_1 and C_2 computed for H^-, together with the experimental T_{2g} peak positions in the D^- samples, were used to calculate Ω. We then calculated the A_{1g} and E_g peak positions. The results are given in lines 7 and 8 of Table II. The calculated E_g peak position agreed favorably with the measured value (line 2), and the ratio between A_{1g} and T_{2g} splittings in the H^-- and D^--doped samples was found to be 2.06 in KI and 2.07 in KBr in excellent agreement with the expected values. The frequencies of the infrared-active localized mode were then calculated for all four samples (line 9). The calculated values are in good agreement with the available experimental data (line 10).

It appears that the static-well approximation gives a good consistent description of the available infrared and Raman-scattering data for U centers in KBr and KI, at least as far as peak positions are concerned. What is probably more important, however, is that the Raman data give a measure of the anharmonicity associated with the localized mode. This information can be used as an addi-

TABLE II. Peak positions and potential-energy parameters for U centers in KBr and KI.

	Source	KI : H^-	KI : D^-	KBr : H^-	KBr : D^-
ω_T (cm^{-1})	this expt	753.1	543.4	886.3	635.0
ω_E (cm^{-1})	this expt	767.9	550.2	904.5	644.4
ω_A (cm^{-1})	this expt	759.9		894.8	
$C_1\left(10^{18}\frac{\text{erg}}{\text{cm}^4}\right)$	calc	5.76		9.86	
$C_2\left(10^{18}\frac{\text{erg}}{\text{cm}^4}\right)$	calc	−13.56		−23.0	
Ω (cm^{-1})	calc	377.8	272.3	444.6	318.2
ω_E (cm^{-1})	calc		550.5		643.8
ω_A (cm^{-1})	calc		546.7		639.1
ω_{ir} (cm^{-1})	calc	379.0	273.0	446.5	319.1
ω_{ir} (cm^{-1})	expt	378[a] 382[b]	?	445[a], 446[b] 447[d], 450[e]	318[c] 319[d]

[a]Reference 1. [c]Reference 11. [e]Reference 33.
[b]Reference 17. [d]Reference 32.

tional test of theoretical models of the defect and its interactions.

V. POTENTIAL ENERGY

In Sec. II the potential energy for the U-center-localized oscillator was written in terms of parameters Ω, C_1, and C_2, which were to be determined by experiment. In this section we discuss the various terms which contribute to the potential. We also use the experimentally determined parameters C_1 and C_2 to determine the repulsive short-range interaction between the U center and its nearest neighbors. These results are then used to calculate the harmonic contribution to the local-mode frequency. The effect of the polarizability of the U center and its neighbors is demonstrated.

There are four contributions to the potential energy which describe the interaction of the U center with the host-crystal ions:

(i) a short-range repulsive interaction arising from the overlap of the U-center electron cloud with the electron distribution of its neighbors. Only the nearest-neighbor ions should be expected to contribute significantly to this interaction. We represent it by a Born-Mayer potential

$$V_{\mathrm{REP}} = A_{\mathrm{REP}} \sum_{nn} e^{-|\vec{r}-\vec{r}_{nn}|/\rho} , \tag{3}$$

where $\vec{r}$ is the position of the U center and the sum is over its nearest neighbors.

(ii) a long-range Coulomb interaction

$$V_{\mathrm{COUL}} = \sum_j \frac{\pm e^2}{|\vec{r}-\vec{r}_j|} . \tag{4}$$

Here the sum is over all the host crystal ions.

(iii) a short-range attractive van der Waals interaction

$$V_{\mathrm{VW}} = -\sum_{nn} \left(\frac{C_{\mathrm{VW}}}{|\vec{r}-\vec{r}_{nn}|^6} + \frac{D_{\mathrm{VW}}}{|\vec{r}-\vec{r}_{nn}|^8} \right) . \tag{5}$$

The first term is an induced dipole-dipole term; the second is a dipole-quadrupole term. We shall include only nearest-neighbor interactions here also. The coefficients C_{VW} and D_{VW} are given by[34]

$$C_{\mathrm{VW}} = \frac{3h}{2} \frac{\nu(\mathrm{H}^-) - \nu(\mathrm{K}^+)}{\nu(\mathrm{H}^-) + \nu(\mathrm{K}^+)} \alpha(\mathrm{H}^-)\,\alpha(\mathrm{K}^+) , \tag{6}$$

$$D_{\mathrm{VW}} = \frac{9h}{4e^2} C_{\mathrm{VW}} \left[\tfrac{1}{2}\nu(\mathrm{H}^-)\alpha(\mathrm{H}^-) + \tfrac{1}{8}\nu(\mathrm{K}^+)\alpha(\mathrm{K}^+) \right] , \tag{7}$$

where the ν's are series-limit frequencies of the discrete spectra of the interacting ions and the α's are their crystal polarizabilities;

(iv) a polarization term. We shall discuss it later.

Therefore the total potential energy (neglecting polarization effects) may be written as

$$V_{\mathrm{TOT}} = V_{\mathrm{REP}} + V_{\mathrm{VW}} + V_{\mathrm{COUL}} . \tag{8}$$

Using this expression for the potential energy, we can determine the repulsive potential parameters ρ and A_{REP} from our Raman data. To do this, we first expand V_{TOT} in a power series in the displacements of the U center from equilibrium keeping terms through fourth order. We obtain

$$V_{\mathrm{TOT}} = Kr^2 + C_1(x^4+y^4+z^4) + C_2(x^2y^2+y^2z^2+z^2x^2) , \tag{9}$$

where

$$K = K_{\mathrm{REP}} + K_{\mathrm{VW}} , \tag{10}$$

$$C_1 = C_{1\,\mathrm{REP}} + C_{1\,\mathrm{COUL}} + C_{1\,\mathrm{VW}} , \tag{11}$$

$$C_2 = C_{2\,\mathrm{REP}} + C_{2\,\mathrm{COUL}} + C_{2\,\mathrm{VW}} \tag{12}$$

in an obvious notation.

Constant terms have been neglected. All odd powers in the expansion and several quadratic and quartic terms vanish because of the O_h symmetry at the U-center site. The Coulomb interaction contributes no quadratic terms since $\nabla^2 V_{\mathrm{COUL}} = 0$. This condition also implies that $C_{2\,\mathrm{COUL}} = -3C_{1\,\mathrm{COUL}}$.

Since the sums in the repulsive and van der Waals interactions have been limited to nearest neighbors of the U center, it is straightforward to obtain the algebraic forms of the expansion coefficients K_{REP}, K_{VW}, $C_{1\,\mathrm{REP}}$, $C_{1\,\mathrm{VW}}$, $C_{2\,\mathrm{REP}}$, and $C_{2\,\mathrm{VW}}$ in terms of the impurity-nearest-neighbor separation a (which may be different from the host-crystal value r_0). These expressions are given in Table III.

Once the repulsive parameters ρ and A_{REP} are determined, the frequency Ω of the high-frequency infrared-active localized mode in the harmonic approximation can be calculated from the relation

$$\tfrac{1}{2}M'\Omega^2 = K , \tag{19}$$

where

$$K = A_{\mathrm{REP}} e^{-a/\rho} \left(\frac{1}{\rho^2} - \frac{2}{\rho a} \right) - \frac{30C_{\mathrm{VW}}}{a^8} - \frac{56D_{\mathrm{VW}}}{a^{10}} . \tag{20}$$

We had some latitude in the choice of the impurity-nearest-neighbor separation a. The best fits to the observed infrared sideband structure[12,13,23] have been made assuming a reduction in the central-force constant between the nearest neighbors of the U center and their nearest neighbors in [100] directions (fourth neighbors of the impurity), as well as a decreased impurity-nearest-neighbor central-force constant. These reductions result in an inward relaxation of the U center's nearest neighbors of a few percent. Quantum-mechanical calculations by Wood and Gilbert[36] yield similar results. Also, the results of x-ray measurements of the lattice constants of KBr doped with U centers have been used by Lüty *et al.*[37] to calculate a 1% inward relaxation of the U center's nearest neighbors. Benedek and Nardelli[38] have calculated a 5% inward relaxation of the nearest neighbors in KI:H^-. How-

TABLE III. Contributions to anharmonic potential-energy coefficients.

	Coulomb	$V=Kr^2+C_1(x^4+y^4+z^4)+C_2(x^2y^2+y^2z^2+z^2x^2)$ Born-Mayer	van der Waals	Polarization
K	0	$A_{\mathrm{REP}}e^{-a/\rho}\left(\frac{1}{\rho^2}-\frac{2}{\rho a}\right)$	$-\frac{30C_{\mathrm{VW}}}{a^8}-\frac{56D_{\mathrm{VW}}}{a^{10}}$	$-\frac{e^2}{2v}\left(\frac{8\pi}{3}\right)\left(\frac{e^*}{e}\right)\frac{\alpha(\mathrm{H}^-)+\alpha(\mathrm{K}^+)}{\alpha(\mathrm{H}^-)+\alpha(\mathrm{K}^+)+3v/8\pi}$
C_1	$\frac{-7e^2}{2a^5}$	$A_{\mathrm{REP}}e^{-a/\rho}\left(\frac{1}{12\rho^4}+\frac{1}{2\rho^2a^2}+\frac{1}{2\rho a^3}\right)$	$-\frac{276C_{\mathrm{VW}}}{a^{10}}-\frac{700D_{\mathrm{VW}}}{a^{12}}$	...
C_2	$\frac{21e^2}{2a^5}$	$A_{\mathrm{REP}}e^{-a/\rho}\left(\frac{1}{\rho^3a}-\frac{3}{2\rho^2a^2}-\frac{3}{2\rho a^3}\right)$	$\frac{272C_{\mathrm{VW}}}{a^{10}}+\frac{560D_{\mathrm{VW}}}{a^{12}}$	...

ever, there seem to be no definitive values of the lattice relaxation about the U center in KBr and KI. We therefore decided to do the calculations with a as a parameter which we allowed to decrease from r_0 in 1% steps up to 6% relaxation of the lattice about the impurity.

Because of the long range of the Coulomb interaction, the expansion coefficients $C_{1\,\mathrm{COUL}}$ and $C_{2\,\mathrm{COUL}}$ contain contributions from all the ions in the lattice. However, we note that the contributions to $C_{1\,\mathrm{COUL}}$ from the four ion shells closest to the impurity are[35]

$$C_{1\,\mathrm{COUL}}(1\mathrm{st}\ nn)=-\frac{7e^2}{2a^5}\ , \tag{13}$$

$$C_{1\,\mathrm{COUL}}(2\mathrm{nd}\ nn)=-\frac{7e^2}{16\sqrt{2}\,a^5}=-0.310\,\frac{e^2}{a^5}\ , \tag{14}$$

$$C_{1\,\mathrm{COUL}}(3\mathrm{rd}\ nn)=+\frac{28}{81\sqrt{3}}\,\frac{e^2}{a^5}=+0.200\,\frac{e^2}{a^5}\ , \tag{15}$$

$$C_{1\,\mathrm{COUL}}(4\mathrm{th}\ nn)=+\frac{7}{64}\,\frac{e^2}{a^5}=+0.109\,\frac{e^2}{a^5}\ . \tag{16}$$

The last three terms effectively add to zero. Therefore, despite the long range of the Coulomb interaction, we shall make only a small error by considering the Coulomb contribution from nearest neighbors alone.

Neglecting polarization effects and using the results of Table III, we may write

$$A_{\mathrm{REP}}\,e^{-a/\rho}\left(\frac{1}{12\rho^4}+\frac{1}{2\rho^2a^2}+\frac{1}{2\rho a^3}\right)=C_1+\frac{7e^2}{2a^5}+\frac{276C_{\mathrm{VW}}}{a^{10}}+\frac{700D_{\mathrm{VW}}}{a^{12}}\ , \tag{17}$$

$$-A_{\mathrm{REP}}\,e^{-a/\rho}\left(\frac{1}{\rho^3a}+\frac{3}{2\rho^2a^2}+\frac{1}{2\rho a^3}\right)=C_2-\frac{21e^2}{2a^5}-\frac{272C_{\mathrm{VW}}}{a^{10}}-\frac{560D_{\mathrm{VW}}}{a^{12}}\ . \tag{18}$$

C_1 and C_2 are known from our Raman data. C_{VW} and D_{VW} can be calculated from (6) and (7) using the input parameters of Table IV. Thus, if the impurity-nearest-neighbor separation a is known, (17) and (18) constitute two simultaneous equations in the two unknown parameters ρ and A_{REP}. These equations can be solved numerically on the computer.

When these calculations were performed, the resulting values of Ω were 15–20% too high, as shown in the last two columns of Tables V and VI. We attributed this to neglect of polarization effects.

When the impurity undergoes a displacement $\vec{u}$ from its equilibrium position, a dipole of strength $-e\vec{u}$ is created. Within the framework of the adiabatic approximation, this is a static-dipole moment; it induces dipoles on the surrounding ions in proportion to their polarizabilities. These induced dipoles produce an electric field at the position of the impurity which tends to pull it farther away from its equilibrium position. In reality, the impurity-induced dipoles on the nearest-neighbor ions also polarize ions farther removed from the impurity; the polarization of these ions then affects the dipole moments of the nearest neighbors which in turn affect the electric field at the impurity site. Clearly, a self-consistent calculation is required to properly describe these affects. We have not attempted such a calculation here, but have attempted to include polarization effects as an *ad hoc*

TABLE IV. Input parameters for repulsive potential calculation.

	r_0(Å)[a] (0 K values)	ρ_0 (Å)[a]	A_0[b] (10^{-9} erg)	$\alpha(\mathrm{H}^-)$[c]	$\alpha(\mathrm{K}^+)$[a] (10^{-24} cm^3)	α(halide$^-$)[a]	$\nu(\mathrm{H}^-)$[c]	$\nu(\mathrm{K}^+)$[c] (10^{15} cps)	Ω[d] (10^{13} rad/sec)
KBr	3.2658	0.3192	5.58	1.864	1.201	4.130	2.13	5.75	8.37
KI	3.4918	0.3305	7.08	1.864	1.201	6.199	2.13	5.75	7.12

[a]Reference 38.
[b]Calculated from 0 K values of r_0 and ρ_0 using equilibrium condition.
[c]Reference 36.
[d]Fit to our Raman data.

TABLE V. Results of repulsive potential calculation for KI:H⁻.

nn Dist (Å)	Extremal values ρ_{max} (Å)	ρ_{min} (Å)	$A_{REP\ max}$ (10^{-9} erg)	$A_{REP\ min}$ (10^{-9} erg)	ρ (Å)	Best fits (including polarization) A_{REP} (10^{-9} erg)	Ω (10^{13} rad/sec)	% dev.	Best fits (no polarization) Ω (10^{13} rad/sec)	% dev.
3.492	0.724	0.629	0.1065	0.0792	0.713	0.0827	6.88	−3.4	8.53	19.7
3.457	0.718	0.628	0.1058	0.0800	0.699	0.0848	6.85	−3.8	8.61	21.0
3.422	0.702	0.618	0.1079	0.0824	0.693	0.0847	6.82	−4.2	8.71	22.3
3.387	0.686	0.609	0.1103	0.0851	0.686	0.0851	6.78	−4.7	8.79	23.4
3.352	0.670	0.598	0.1121	0.0881	0.670	0.0881	6.74	−5.3	8.87	24.5
3.317	0.641	0.588	0.1163	0.0952	0.641	0.0961	6.69	−6.1	8.95	25.8
3.282	0.638	0.588	0.1157	0.0952	0.638	0.0952	6.64	−6.7	9.06	27.2

correction to the impurity-nearest-neighbor central-force constant as described below.

We first remark that there seems to be no easy way to include the effects of polarization on the quartic coefficients C_1 and C_2. The one-dimensional calculation of Matthew[35] indicates that the size of the polarization contribution to these coefficients would be about 10–15% of the Coulomb contribution. To at least partially account for these effects, and for experimental error in determining the quartic coefficients, we have allowed C_1 and C_2 to vary in these calculations by ±15% from the experimentally determined value.

We included polarization effects in the calculation of the local-mode frequency Ω by including in the quadratic coefficient K a contribution K_{POL} given by

$$K_{POL} = -\frac{e^2}{2v}\left(\frac{8\pi}{3}\right)\frac{\alpha(H^-)+\alpha(K^+)}{\alpha(H^-)+\alpha(K^+)+3v/8\pi}\ , \qquad (21)$$

where $v = 2a^3$. This term, due to Behedek and Nardelli,[38,39] is essentially the polarization contribution to the effective impurity-nearest-neighbor central-force constant. We then had

$$\tfrac{1}{2}M'\Omega^2 = A_{REP}\,e^{-a/\rho}\left(\frac{1}{\rho^2}-\frac{2}{\rho a}\right) - \frac{30C_{VW}}{a^8} - \frac{56D_{VW}}{a^{10}} + K_{POL}\ . \qquad (22)$$

The results of this calculation are presented in Tables V and VI. When polarization effects are included, the calculated local-mode frequency for KI:H⁻ for 0–6% relaxation agrees quite well with the experimental value of 7.12×10^{13} rad/sec. The best fit for KBr:H⁻, which also occurs for no relaxation, is about 10% lower than the experimental value of 8.37×10^{13} rad/sec, and the calculated frequency gets progressively smaller as the inward relaxation is increased. For a given nearest-neighbor separation, the values of ρ vary as a function of C_1 and C_2 by at most 16% for both KBr and KI, whereas the variation in A_{REP} is up to 40% for KBr and 25% for KI. The worst frequency fits as a function of C_1 and C_2 are typically 8% worse than the best fits for KBr; for KI this figure is about 7%.

The Benedek-Nardelli expression from which we obtained K_{POL} actually contained a factor $(e^*/e)^2$, where e^* is an effective charge. Throughout our calculations we have taken e^* equal to the bare electronic charge. Fritz[16] has estimated that e^* should be about $0.8e$ for U centers. All other things being equal, a decrease in effective charge would decrease the effect of the polarization term and increase the calculated frequency. This is what is needed for KBr and, to a lesser extent, for KI. However, the Coulomb and van der Waals terms would also be affected by a change in effective charge, and these terms affect the calculation

TABLE VI. Results of repulsive potential calculation for KBr:H⁻.

nn Dist (Å)	Extremal values ρ_{max} (Å)	ρ_{min} (Å)	$A_{REP\ max}$ (10^{-9} erg)	$A_{REP\ min}$ (10^{-9} erg)	ρ (Å)	Best fits (including polarization) A_{REP} (10^{-9} erg)	Ω (10^{13} rad/sec)	% dev.	Best fits (no polarization) Ω (10^{13} rad/sec)	% dev.
3.266	0.648	0.558	0.1446	0.1019	0.648	0.1019	7.49	−10.5	9.55	14.1
3.233	0.633	0.549	0.1468	0.1057	0.633	0.1057	7.42	−11.3	9.61	14.8
3.200	0.602	0.539	0.1524	0.1147	0.594	0.1213	7.32	−12.6	9.68	15.7
3.168	0.595	0.524	0.1616	0.1184	0.595	0.1184	7.25	−13.4	9.75	16.4
3.135	0.580	0.520	0.1629	0.1239	0.580	0.1239	7.16	−14.5	9.84	17.5
3.103	0.547	0.525	0.1553	0.1373	0.547	0.1408	6.92	−17.3	9.96	19.0
3.070	0.544	0.500	0.1770	0.1399	0.544	0.1399	6.83	−18.4	10.04	19.9

of the Born-Mayer parameters. In view of the uncertainty in the relaxation of the U-center's nearest neighbors and our other approximations, it did not seem worthwhile to introduce any other variable parameters.

Several authors[6,7,34] have represented the short-range interaction between the U center and its neighbors by a Huggins-Mayer potential, in which only the ionic radius of the H^- ion differentiated the U center from the halide ion for which it substituted. Using this model, Striefler and Jaswal[34] calculated the local-mode frequency for H^- ions in KBr and obtained reasonable agreement with experimental results. However, if one uses the same parameters to calculate the values of C_1 and C_2, using our values for the Coulomb and van der Waals contribution to these terms, one obtains

$$C_1 \approx +15\times10^{18}\ \text{erg/cm}^4\,, \quad C_2 \approx +20\times10^{18}\ \text{erg/cm}^4\,.$$

Not only are the relative magnitudes of C_1 and C_2 in disagreement with the experimentally determined values (cf. Table II), but the sign of C_2 is incorrect. Our results indicate that a better approximation is to use the screening parameter ρ for the appropriate alkali hydride.

Our calculations also predict decreases in the repulsive potential contribution to the central-force constant between the U center and its nearest neighbors; however, these decreases are of the order of 20%, whereas more sophisticated models, which give excellent agreement with experiment, predict decreases of about 50%.

The importance of the polarization contribution to the nearest-neighbor force constant is evident from our results. This is especially true in KI, where the best calculation of the local-mode frequency without polarization is 20% too high.

Recently, Singh and Mitra[40] calculated the impurity-nearest-neighbor central-force constants for U and F centers in alkali halides including KBr and KI. They used the molecular model of Jaswal[41] and included polarization effects in a similar but not identical manner to ours. Differences in input parameters make detailed comparison with our work difficult, but basically the two sets of results are in reasonable agreement.

VI. EXPERIMENTAL RESULTS AND DISCUSSION–LOW-FREQUENCY REGION

We have also studied the low-frequency band-mode region of KI: H^- in an effort to observe the even-parity configurations which give rise to sidebands of the local mode. Recent in-depth studies by MacPherson and Timusk[12,13] indicate the presence of an incipient resonance of E_g symmetry at 31 cm^{-1}, an E_g resonance mode at 65 cm^{-1}, and a gap mode at 93.5 cm^{-1}. Stress measurements by Fritz *et al.*[16] assign A_{1g} symmetry to this gap mode. In our Raman measurements, we were unable to see either the 31- or the 65-cm^{-1} bands. We also failed to observe any structure which could be attributed to defect-activated critical points in the one-phonon density of states. We estimate that at least a tenfold increase in impurity concentration would be needed to observe these features.

To determine the presence or absence of the A_{1g} gap mode, one needs to subtract the two-phonon scattering from the host crystal. Unfortunately, relative to the effects of the H^-, this scattering is quite strong even at low temperatures. As in the case of the second harmonics, the data in the band-mode region were taken point by point at 0.2-Å intervals with 100-sec dwell time at each point. At this slow rate of data acquisition, the pure and the doped samples had to be run on different days, and it was found that the intensity obtained from the pure crystal was three to four times greater than that obtained in the doped sample. This was probably due to the far sharper focusing of the incident laser beam in the pure crystal. Nevertheless, there appeared to be a definite difference in the shapes of the pure- and doped-crystal spectra in the region near 95 cm^{-1} where the A_{1g} gap mode was observed in the sideband studies. To facilitate further comparison, we scaled the $z(xx)y$ spectrum of KI: H^- to the measured spectrum of the pure-host KI crystal in the regions 50–85 and 105–125 cm^{-1}, i.e., on both sides of the possible impurity peak but far enough from it that it would not influence the fitting.

The Raman intensities of the pure and doped crystals in the $z(xx)y$ geometry are plotted in Fig. 4. The ordinate is Raman efficiency obtained by comparison with that of benzene (see below). The presence of a sharp peak at about 95 cm^{-1} in the doped sample is clearly evident. Since no impurity-induced T_{2g} or E_g scattering was observed, this peak must have A_{1g} symmetry. We attribute it to Raman scattering by the gap mode previously observed in infrared sideband measurements.

VII. ABSOLUTE RAMAN EFFICIENCIES AND CROSS SECTIONS

In the case of KI: H^- we have measured the absolute Raman efficiencies and differential cross sections of each of the three second-harmonic lines by comparison with benzene. Details of the measurement are given in the Appendix, and the results are presented in Table VII.

The frequency-integrated Raman efficiency for the A_{1g} gap mode is directly obtainable from the area under the 95-cm^{-1} peak in the difference of the two curves in Fig. 4. Its value is given in Table VII together with the differential cross section.

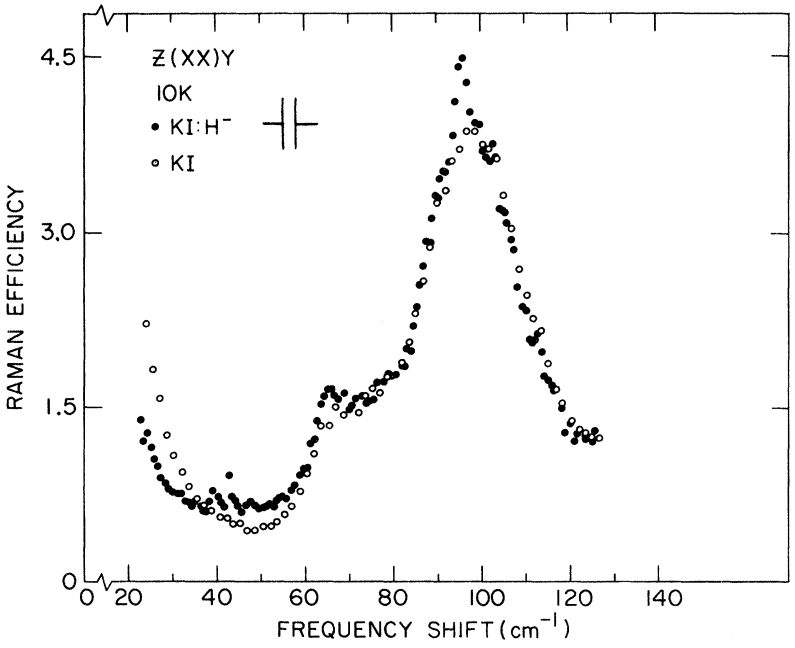

FIG. 4. $z(xx)y$ Raman spectra of KI : H⁻ and pure KI at low frequency. $x \parallel [110]$, $y \parallel [\bar{1}10]$, and $z \parallel [001]$. Open circles: pure KI; filled circles: KI : H⁻. Raman efficiency is in units of (10^{-12}/ cm sr cm^{-1}) and frequency is measured in wave-number units.

The magnitude of the differential cross section can be used to estimate the polarizability derivative associated with the gap mode. The frequency-integrated differential Raman cross section for an impurity mode of A_{1g} symmetry may be written[42]

$$\frac{d\sigma_A}{d\Omega} = \left(\frac{\omega_s}{c}\right)^4 \left(\frac{\hbar}{2\omega_A M}\right) \left|\frac{\partial P_{gg}}{\partial u_A}\right|^2 [\bar{n}(\omega_A)+1] \,. \tag{23}$$

Here u_A is the linear combination of atomic displacements comprising the dynamical coordinate for the A_{1g} breathing mode,[43] M is the mass of a nearest neighbor of the impurity, and $\bar{n}(\omega_A)$ is the thermal occupation number for a harmonic oscillator of frequency ω_A. In this expression we have made the reasonable approximation that the gap mode may be treated as an independent Einstein oscillator so that the perturbed density of states which appears in a rigorous expression for the frequency-dependent cross section[42] reduces to a δ function.

From this expression, and the value of the cross section given in Table VII we obtain

$$\left|\frac{\partial P_{gg}}{\partial u_A}\right| = 1.16\times10^{-16} \text{ cm}^2 \,. \tag{24}$$

By symmetry,

$$\frac{\partial P_{xx}}{\partial u_A} = \frac{\partial P_{yy}}{\partial u_A} = \frac{\partial P_{gg}}{\partial u_A} \tag{25}$$

and

$$\frac{\partial P_{ij}}{\partial u_A} = 0 \quad \text{for } i \neq j \,. \tag{26}$$

VIII. ADDITIONAL REMARKS

The first-order Raman scattering by the A_{1g} gap mode and the two-quantum scattering by the three second-harmonic levels of the high-frequency localized mode in KI: H⁻ have been observed to be comparable in strength (cf. Table VII), whereas one generally expects that first-order scattering, when allowed by symmetry, should be considerably stronger. A possible explanation for this situation may come from the fact that the H⁻ ion is similar to the halide ions in electronic structure. First-order Raman scattering results from a vibration-induced first-order change in electronic polarizability. In the pure alkali halide crystals, such first-order changes are identically zero, and no first-order scattering is observed. On the other hand, second-order polarizability changes are nonzero in the pure crystal. Apparently the U center represents too weak an electronic perturbation to produce a large first-order polarizability change; nevertheless, it can induce second-order polar-

TABLE VII. Absolute Raman efficiencies and differential cross sections for H⁻ ions in KI for 4880-Å exciting light.

	Second harmonics			Gap mode
	T_{2g}	A_{1g}	E_g	(A_{1g})
Raman efficiency (cm sr)$^{-1}$	2.23×10^{-12}	9.06×10^{-13}	1.33×10^{-12}	1.11×10^{-12}
Differential cross section (cm^2/sr)	3.33×10^{-30}	1.35×10^{-30}	1.99×10^{-30}	1.66×10^{-30}

izability changes analogous to those caused by host-crystal halide ions because its electronic structure is similar to theirs. This explanation is consistent with the fact that the only impurities known to produce strong first-order Raman scattering in the alkali halides are Tl^+,[44,45] Ag^+,[42,46,47] and Cu^+,[48,49] which are all quite different electronically from the ions they replace and so can be expected to introduce large electronic perturbations.

The relative intensities of the second-harmonic peaks (Table VII) remain a puzzle. We have attempted several calculations of the relative Raman intensities using expressions for the electron-lattice coupling which are linear, quadratic, or both in the displacements of the U center from equilibrium. All these calculations have predicted that the $A_{1g}+E_g$ scattering should be considerably stronger than the T_{2g} scattering. This is in direct contradiction to our experimental results. Any light that could be shed on this problem would be welcome.

ACKNOWLEDGMENTS

The authors are indebted to Ross Freeman for his automation of the photon-counting electronics and to Mrs. J. Peascoe for taking some of the KI data for the absolute cross-section measurements.

APPENDIX—ABSOLUTE RAMAN EFFICIENCIES AND CROSS SECTIONS: EXPERIMENTAL DETAILS

The absolute measurements were performed in a manner similar to that used earlier by Johnston and Kaminow for Raman line spectra.[50] With continuous Raman spectra some changes must be made. These techniques will now be discussed.

The Raman power per unit frequency range at frequency ω scattered into solid angle Ω at the monochromator entrance slit is given by

$$P_R(\omega)=(P_L/\text{area of beam at sample})\frac{d\sigma(\omega)}{d\Omega}\frac{\Omega}{n^2}NTV\,, \tag{A1}$$

where P_L is the output laser power; N is the number of scattering centers per unit volume; V is the volume of the laser beam in the sample which is equal to the (cross sectional area of beam)$\times$(interaction length l of beam with sample); T is the transmission factor, which takes into account losses due to optical components, reflection from sample surfaces, etc.; n is the index of refraction of the sample; and $d\sigma(\omega)/d\Omega$ is the frequency-dependent differential-scattering cross section. The measured Raman signal at frequency ω is

$$S(\omega)=(l_m/l)\,D(\omega)\int P_R(\omega')\,I(\omega-\omega')\,d\omega\,. \tag{A2}$$

Here l_m/l is the fraction of the beam-sample interaction length for which light is collected by the monochromator and $D(\omega)$ is a throughput factor for the monochromator and photomultiplier tube combination at frequency ω [measured in A/W or (counts/sec)W^{-1}]. The factor $\int P_R(\omega')I(\omega-\omega')\,d\omega'$ represents the fact that the measured spectrum is a convolution of the true Raman line shape with the instrument profile $I(\omega-\omega')$ of the spectrometer.

We define the Raman efficiency at frequency ω (sometimes referred to as Raman efficiency per unit length) by the relation

$$R(\omega)=N\frac{d\sigma(\omega)}{d\Omega}\,. \tag{A3}$$

Then we may write

$$S(\omega)=K\int R(\omega')\,I(\omega-\omega')\,d\omega'\,, \tag{A4}$$

with

$$K=D(\omega)P_L\,Tl_m\Omega/n^2\,. \tag{A5}$$

We assume that $D(\omega)$ may be treated as a constant over a limited frequency range such as that spanned by the three second-harmonic peaks or the gap-mode region in KI:H^-. (Of course the value of the constant differs in the two different spectral regions.)

The quantity $I(\omega-\omega')$, which may be obtained by scanning through the laser line, is sharply peaked about $\omega'=\omega$. Hence, if we are dealing with a continuous spectrum such as the two-phonon spectrum in KI, we note that the integral in (A4) will have an appreciable value only for $\omega'\approx\omega$; in such a case we may write

$$S(\omega)=KR(\omega)\,A_{\text{inst}}\,, \tag{A6}$$

where $A_{\text{inst}}=\int I(\omega-\omega')\,d\omega'$ is the area under the instrument profile of the spectrometer. For any Raman line, we may integrate relation (A4) over ω; with the aid of a simple change of variable, this yields

$$\int S(\omega)\,d\omega=KRA_{\text{inst}}\,, \tag{A7}$$

where $R=\int R(\omega)\,d\omega$ which is the frequency-integrated Raman efficiency associated with the given Raman line. In the special case of the continuum, integration of (A6) over ω gives the same result.

Using the above expressions, we were able to obtain the Raman efficiencies and cross sections for the impurity modes in KI:H^- by the following procedure. (In what follows quantities referring to the KI two-phonon spectrum, impurity spectra, and benzene are subscripted KI, H, and B, respectively.) At the time that each impurity spectrum was taken, the room-temperature two-phonon spectrum of the host KI crystal was recorded under identical experimental conditions. Thus all effects of the spectrometer [except possibly $D(\omega)$ which was determined with the aid of a standard lamp], all transmission factors, and all geometrical factors were the same in both sets of measurements. Then, application of (A7) to both spectra gives

$$\int S_H(\omega)\,d\omega \Big/ \int S_{KI}(\omega)\,d\omega$$

$$= D(\omega_H) \int R_H(\omega)\,d\omega \Big/ D(\omega_{KI}) \int R_{KI}(\omega)\,d\omega$$

$$= \frac{R_H}{R_{KI}} \frac{D(\omega_H)}{D(\omega_{KI})} \cdot \quad \text{(A8)}$$

At a later date we measured the Raman spectrum of the 992-cm^{-1} line of benzene for which absolute cross-section measurements have been made.[51,52] We then replaced the benzene cell with the KI crystal and, under the same experimental conditions, we again measured the KI two-phonon spectrum. In these measurements special care was taken to ensure that the image of the laser beam in the samples was completely contained within the spectrometer slits, so that scattered light from samples illuminated by the entire width of the laser beam would enter the monochromator. The lengths of the benzene cell and the crystal were sufficiently large that light from the same interaction length in both materials was collected by the spectrometer. From these measurements, we obtained the result

$$\int S_B(\omega)\,d\omega \Big/ \int S'_{KI}(\omega)\,d\omega = \frac{K_B}{K_{KI}} \left[\int R_B(\omega)\,d\omega \Big/ \int R_{KI}(\omega)\,d\omega \right]$$

$$= \frac{R_B D(\omega_B) T_B n_{KI}^2}{R_{KI} D(\omega_{KI}) T_{KI} n_B^2} \cdot \quad \text{(A9)}$$

(Here we have denoted the KI two-phonon spectrum by a prime to distinguish it from the two-phonon signal measured at the same time as the impurity spectra.)

Using (A8) and (A9) to eliminate the quantity $D(\omega_{KI})\,R_{KI}$, we obtain

$$R_H = \left[\int S_H(\omega)\,d\omega \Big/ \int S_B(\omega)\,d\omega \right]$$

$$\times \left[\int S'_{KI}(\omega)\,d\omega \Big/ \int S_{KI}(\omega)\,d\omega \right] \frac{T_B D(\omega_B) n_{KI}^2}{T_{KI} D(\omega_H) n_B^2} R_B \cdot \quad \text{(A10)}$$

This expression was used to determine the absolute Raman-scattering efficiencies of the second harmonics in KI : H^-.

To find the gap-mode efficiency in KI : H^- we found it convenient to use the frequency-dependent Raman efficiency of the host KI crystals. Measurements of the KI two-phonon spectrum were made at room temperature and at 10 K under otherwise identical experimental conditions. Applying (A6) and (A7) to the room-temperature signal, and using (A9), we find that

$$R_{KI}(\omega) = S_{KI}(\omega) \left\{ \left[R_B \Big/ \int S_B(\omega)\,d\omega \right] \right.$$

$$\left. \times \left[\int S'_{KI}(\omega)\,d\omega \Big/ \int S_{KI}(\omega)\,d\omega \right] \frac{T_B D(\omega_B) n_{KI}}{T_{KI} D(\omega_{KI}) n_B^2} \right\} \cdot \quad \text{(A11)}$$

The quantity in brackets was used as a multiplicative factor to convert the low-temperature signal to an absolute efficiency.

The room-temperature Raman efficiency is, of course, directly obtainable from the signal $S'_{KI}(\omega)$ taken at the same time as the benzene spectrum:

$$R_{KI}(\omega) = \left[S'_{KI}(\omega) \Big/ \int S_B(\omega)\,d\omega \right] \frac{T_B D(\omega_B) n_{KI}^2}{T_{KI} D(\omega_{KI}) n_B^2} R_B \cdot \quad \text{(A12)}$$

The values of $R_{KI}(\omega)$ obtained from (A11) and (A12) were compared and found to agree to within 2% at all frequencies.

In our computations we determined R_B from the absolute cross-section measurements of Kato and Takuma.[52] These authors measured the frequency-integrated cross section of the 992-cm^{-1} benzene line directly. Since this quantity is directly proportional to R_B, we felt that their measurement was more applicable to our calculations than the measurements of Skinner and Nilsen[51] who measured the peak cross section and linewidth of the 992-cm^{-1} line. To use their results, we would have had to make assumptions about the line shape in order to arrive at the frequency-integrated Raman efficiency R_B.

Many of the uncertainties which are often present in absolute cross-section measurements arise from geometrical considerations. These sources of error are eliminated in our measurements because the geometrical factors cancel out when we take ratios of measured signals. The major source of error in these measurements arises from our inability to determine precisely the baselines in our experimental spectra. This is especially true in the low-temperature impurity spectra which are very weak and show large fluctuations. We estimate that the efficiencies and cross sections presented in Table VII are accurate to within at least 25%.

---

†Work supported by National Science Foundation under Contracts No. GP 6581 and GP 11173 and by Advanced Research Projects Agency, under Contract No. HC 15-67-C-0221.

*Present address: Code 6512, U. S. Naval Research Laboratory, Washington, D. C. 20390.

‡Present address: The Aerospace Corp., P. O. Box 95058, Los Angeles, Calif. 90045.

[1] G. Schaefer, J. Phys. Chem. Solids 2, 233 (1960).

[2] H. Rosenstock and C. Klick, Phys. Rev. 119, 1198

(1960).
[3]R. Wallis and A. A. Maradudin, Progr. Theor. Phys. (Kyoto) 24, 1055 (1960).
[4]S. Takeno, S. Kashirvamura, and E. Tenamoto, Progr. Theor. Phys. (Kyoto) Suppl. 23, 124 (1962).
[5]S. S. Jaswal and D. J. Montgomery, Phys. Rev. 135, A1257 (1964).
[6]R. Fieschi, G. F. Nardelli, and N. Terzi, Phys. Rev. 138, A203 (1965).
[7]R. Fieschi, G. F. Nardelli, and N. Terzi, Phys. Letters 12, 290 (1964).
[8]J. B. Page, Jr. and D. Strauch, Phys. Status Solidi 24, 469 (1967).
[9]B. Fritz, in *Lattice Dynamics*, edited by R. F. Wallis (Pergamon, London, 1964).
[10]R. J. Elliott, W. Hayes, G. D. Jones, H. F. Macdonald, and C. T. Sennett, Proc. Roy. Soc. (London) A289, 1 (1965).
[11]T. Timusk and M. V. Klein, Phys. Rev. 141, 664 (1966).
[12]R. MacPherson, Ph.D. dissertation (McMaster University, 1970) (unpublished).
[13]R. MacPherson and T. Timusk, Can. J. Phys. 48, 2176 (1970).
[14]J. B. Page, Jr. and B. G. Dick, Phys. Rev. 163, 910 (1967).
[15]J. B. Page, Jr. and D. Strauch, in *Localized Excitations in Solids*, edited by R. F. Wallis (Plenum, New York, 1968).
[16]B. Fritz, J. Gerlach, and U. Gross, in *Localized Excitations in Solids*, edited by R. F. Wallis (Plenum, New York, 1968).
[17]B. Fritz, U. Gross, and D. Bäuerle, Phys. Status Solidi 11, 231 (1965).
[18]H. Bilz, D. Strauch, and B. Fritz, J. Phys. Radium Suppl. 27, 3 (1966).
[19]D. Bäuerle and B. Fritz, Phys. Status Solidi 24, 207 (1967).
[20]Y. Brada and S. S. Mitra, Bull. Am. Phys. Soc. 9, 644 (1964).
[21]S. S. Mitra and Y. Brada, Phys. Letters 17, 19 (1965).
[22]H. Dötsch, W. Gebhardt, and C. Martius, Solid State Commun. 3, 297 (1965).
[23]T. Gethins, T. Timusk, and E. Woll, Phys. Rev. 157, 744 (1967).
[24]Nguyen Xuan Xinh, Phys. Rev. 163, 896 (1967).
[25]Nguyen Xuan Xinh, Solid State Commun. 4, 9 (1966).
[26]Nguyen Xuan Xinh, A. A. Maradudin, and R. A. Coldwell-Horsfall, J. Phys. Radium 26, 717 (1965).
[27]C. T. Sennett, J. Phys. Chem. Solids 26, 1097 (1965).
[28]J. A. Harrington, R. T. Harley, and C. T. Walker, Solid State Commun. 8, 407 (1970).
[29]R. L. Rosenbaum, Rev. Sci. Instr. 39, 890 (1968).
[30]R. L. Rosenbaum, Rev. Sci. Instr. 40, 577 (1969).
[31]T. Damen, S. P. S. Porto, and B. Tell, Phys. Rev. 142, 570 (1966).
[32]D. Mirlin and I. Reshina, Fiz. Tverd. Tela 6, 3078 (1964) [Sov. Phys. Solid State 6, 2454 (1964)].
[33]A. Mitsuishi and H. Yoshinaga, Progr. Theor. Phys. (Kyoto) Suppl. 23, 241 (1962).
[34]M. Striefler and S. Jaswal, J. Phys. Chem. Solids 30, 827 (1969).
[35]J. A. D. Matthew, Technical Report No. 373, Materials Science Center, Cornell University, 1965 (unpublished).
[36]R. Wood and R. Gilbert, Phys. Rev. 162, 746 (1967).
[37]F. Lüty, S. Mascarenhas, and C. Ribeiro, Phys. Rev. 168, 1080 (1968).
[38]G. Benedek and G. Nardelli, in *Proceedings of the Conference on Calculations of the Properties of Vacancies and Interstitials*, Natl. Bur. Std. Misc. Publ. No. 287 (U. S. GPO, Washington, D.C., 1967).
[39]G. Benedek and G. F. Nardelli, Phys. Rev. 155, 1004 (1967).
[40]R. Singh and S. S. Mitra, Phys. Rev. B 2, 1070 (1970).
[41]S. S. Jaswal, Phys. Rev. 140, A687 (1965).
[42]G. Paul Montgomery, Jr., Ph. D. dissertation (University of Illinois, Urbana, 1971) (unpublished).
[43]M. V. Klein, in *Physics of Color Centers*, edited by W. B. Fowler (Academic, New York, 1968), Chap. 7.
[44]R. T. Harley, J. B. Page, Jr., and C. T. Walker, Phys. Rev. Letters 23, 992 (1962).
[45]R. T. Harley, J. B. Page, Jr., and C. T. Walker, Phys. Rev. B 3, 1365 (1971).
[46]R. Kaiser and W. Möller, Phys. Letters 28A, 619 (1969).
[47]W. Möller, R. Kaiser, and H. Bilz, Phys. Letters 32A, 171 (1970).
[48]G. P. Montgomery, Jr. and R. D. Kirby, in *Light Scattering in Solids*, edited by M. Balkanski (Flammarion, Paris, 1971).
[49]B. N. Ganguly, R. D. Kirby, M. V. Klein, and G. P. Montgomery, Jr., Phys. Rev. Letters 28, 307 (1972).
[50]W. D. Johnston, Jr. and I. P. Kaminow, Phys. Rev. 168, 1045 (1968).
[51]J. G. Skinner and W. G. Nilsen, J. Opt. Soc. Am. 58, 113 (1968).
[52]Y. Kato and H. Takuma, J. Opt. Soc. Am. 61, 347 (1971).